Journal of Materials Chemistry

PAPER

Highly selective acetone fluorescent sensors based on microporous Cd(ii) metal–organic frameworks†

Fei-Yan Yi, Weiting Yang and Zhong-Ming Sun*

Solvothermal reaction of Cd^{2+} ions and a hexavalent carboxylic acid (**H₆L**) afforded a Cd(ii) metal organic framework (Cd-MOF), namely $\{[Cd_3(L)(H_2O)_2(DMF)_2]\cdot 5DMF\}_n$ (**1**). Its structure consists of trinuclear Cd^{II} building units, which are further bridged by the carboxylic ligand, resulting in a 4,4-connected topological net (**sra**). By introducing a rigid N-donor ligand 1,4-bis(1-imidazolyl)benzene (**dib**), a new Cd-MOF (**2**) $\{[Cd_3(L)(dib)]\cdot 3H_2O\cdot 5DMA\}_n$ was isolated, in which the coordinated sites of solvent molecules in **1** were completely replaced by **dib**. The resulting trinuclear Cd_3 subunits are further bridged into a two-fold interpenetrating network with DMA and water molecules located in the void space. The luminescent properties of the two microporous Cd-MOFs dispersed in different solvents have been investigated systematically, demonstrating unique selectivity for the detection of acetone *via* a fluorescence quenching mechanism. Their luminescence intensities decreased to 50% at an acetone content of 0.3 vol% and were almost completely quenched at a concentration of 1.0 vol%, thus, they can be considered as excellent potential luminescent probes for the detection of acetone.
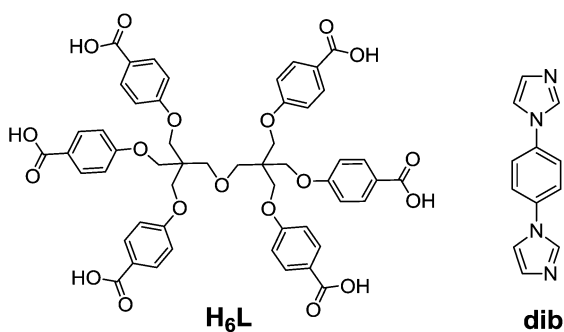
1 Introduction

Molecular recognition is a common phenomenon in the natural world.[1,2] The recognition occurs when two or more molecules exhibit molecular complementarity, including geometrical, chemical, or structural matching. In host–guest chemistry, the "recognition" has been widely used according to the intermolecular host–guest interaction. There is a strong need to develop the recognition phenomena for sensing systems and devices, which possess the ability of rapidly detecting chemicals, even in biological environments. In all sensing types, fluorescent sensing has received the most attention due to its short response time, excellent sensitivity, simplicity and low cost.[3,4] This technique has been used to detect all kinds of small molecules,[5–7] especially volatile organic solvent molecules (VOSMs). Such VOSMs with high toxicity greatly harm our wellbeing, as well as the environment around us. VOSMs also contribute to climate change and destruction of the ozone layer. It becomes an urgent scientific objective to develop new fluorescence sensors for the detection of VOSMs. Up to now, from a large amount of publications devoted to this field, it has been found through fluorescent sensing that most VOSMs are explosives, such as TNT (2,4,6-trinitrotoluene), DNT (2,4-dinitrotoluene) and the principal

ingredients of explosives. Small molecule sensing performance levels, such as selectivity and sensitivity, mainly rely on the naked interaction between the host and the guest, and this interaction is highly affected by solvent, hydrogen bonding capability, π–π stacking and electrostatic interaction. Microporous metal–organic frameworks (MMOFs) with fascinating topologies, large pore sizes, high apparent surface areas and stability of the structures, will be an optimal selection.

Metal–organic frameworks (MOFs) as a new class of crystalline materials have been of significant interest for their functional properties and potential applications in materials science.[8–11] Except playing important roles in gas storage and separation, heterogeneous catalysis and drug delivery, their sensing property will be more explored in the future. MOFs are constructed from metal ions and bridging organic linkers.[12] The adopting metal ions or clusters aid the process of structure prediction, but successful prediction of the target framework relies heavily on the organic links. The size and the chemical environment of the resulting void spaces are also defined by the lengths and functionalities of the organic units, so it is extremely important to select an appropriate organic linker to construct porous MOFs. One effective way to increase the porosity is by extending the size of the ligand. However, extending the size of the ligand may lead to interpenetration of the framework and/or partial collapse of the framework upon guest molecule removal. It is known that interpenetration will decrease the free volume and increase the framework densities, or even diminish the porosity by a high degree of interpenetration. On the other hand, interpenetration can also be used to precisely adjust the pore size and surface area to promote more favorable MOF–guest interactions, such as

State Key Laboratory of Rare Earth Resource Utilization, Changchun Institute of Applied Chemistry, Chinese Academy of Sciences, 5625 Renmin Street, Changchun, Jilin 130022, P.R. China. E-mail: szm@ciac.jl.cn; Fax: +86-431-85698041; Tel: +86-431-85262389

This journal is © The Royal Society of Chemistry 2012

J. Mater. Chem., 2012, **22**, 23201–23209 | 23201

Scheme 1 Structures of ligands **H₆L** and **dib**.

enhancing the hydrogen binding with the adsorption centers, and thereafter to improve gas separation and storage abilities. So control of interpenetration in syntheses of MOFs with high porosity becomes a difficult and challenging task. A dual-ligand way, utilizing complementary ligands with two different functions, such as combining a carboxylate ligand with a basic N-donor ligand, is proved to be successful in the synthesis of porous MOFs, because the use of two complementary ligands provides an additional level of control in the framework structure and charge density distribution. For flexible ligands, they are too flexible to maintain their structural geometries during the self-assembly process. However, the flexibility of ligands is essential to produce some structures with particular properties.[13] Once a rigid ligand is introduced, it can strongly direct the metal coordination and strengthen the whole 3-dimensional (3D) framework, while at the same time the properties of flexible ligands remain. So it can efficiently improve the porosity of the resulting structures and support the whole stability of the framework.

Taking advantage of the excellent sensing properties of MOFs and bearing the aforementioned ideas in mind, a semi-rigid ligand hexa[4-(carboxyphenyl)oxamethyl]-3-oxapentane acid (**H₆L**, Scheme 1) was selected as a building block to construct structures. Solvothermal reaction of **H₆L** and Cd^{2+} in a mixed solvent system DMF–H_2O at 85 °C resulted in a novel porous compound **1** $\{[Cd_3(L)(H_2O)_2(DMF)_2]\cdot 5DMF\}_n$ ($P2_1/c$). Introducing a rigid ligand 1,4-bis(1-imidazolyl)benzene (**dib**, Scheme 1), another novel porous framework **2** $\{[Cd_3(L)(dib)]\cdot 3H_2O\cdot 5DMA\}_n$ was isolated in DMA–H_2O at 100 °C. Their formula were confirmed by elemental analyses, single-crystal X-ray diffraction studies and thermogravimetric analyses (TGA). Significant and sensitive fluorescence quenching phenomena were observed in the two Cd-MMOFs when exposed to acetone.[5]

2 Experimental

2.1 Materials and measurements

All chemicals were commercially obtained and used without further purification. **H₆L** was synthesized by a modified procedure previously documented.[14] 1,4-bis(1-imidazolyl)benzene (**dib**) was purchased from Jinan Henghua Sci. & Tec. Co. Ltd. Elemental analyses of C, H and N in the solid samples were performed with a VarioEL analyzer. Thermogravimetric and

differential thermal analysis (TG-DTA) data were recorded on a Thermal Analysis Instrument (SDT 2960, TA Instruments, New Castle, DE) from room temperature to 800 °C with a heating rate of 10 °C min^{-1} under an air atmosphere. Powder X-ray power diffraction (XRD) patterns were performed on a D8 Focus (Bruker) diffractometer with Cu Kα radiation field-emission ($\lambda = 0.15405$ nm, continuous, 40 kV, 40 mA, increment = 0.02°).

The measurements (N_2 and H_2) were performed on ASAP 2020 and Autosorb MP-1 apparatuses. Prior to the measurement, the as-synthesized samples of **1** and **2** were immersed in methanol and dichloromethane alternately. The resulting exchanged samples were then evacuated (10^{-3} Torr) successively at room temperature and 80 °C.

2.2 Syntheses

Synthesis of $\{[Cd_3(L)(H_2O)_2(DMF)_2]\cdot 5DMF\}_n$ **(1).** $Cd(NO_3)_2\cdot 4H_2O$ (0.12 mmol, 37.1 mg) and **H₆L** (0.04 mmol, 39.0 mg) in a mixed solvent of dimethylformamide (DMF, 6 mL) and distilled water (H_2O, 1 mL) were placed in a Teflon-lined stainless steel vessel (20 mL) and heated to 85 °C in 300 min, maintained at this temperature for three days and then cooled to room-temperature at a rate of 0.2 °C min^{-1}. The resulting colorless crystals were obtained, after being washed by distilled water, yield 59.2 mg (80% based on Cd^{2+}). Its purity was confirmed by X-ray powder diffraction (XRD). Anal. calcd (%) for **1** $C_{73}H_{89}N_7O_{28}Cd_3$ ($M_r = 1849.75$): C, 47.40; H, 4.85; N, 5.30. Found: C, 48.05; H, 4.73; N, 5.21.

Synthesis of $\{[Cd_3(L)(dib)]\cdot 3H_2O\cdot 5DMA\}_n$ **(2).** Compound **2** was synthesized by a procedure similar to that used for **1**, by adding the second auxiliary ligand (**dib**). $Cd(NO_3)_2\cdot 4H_2O$ (0.12 mmol, 37.1 mg), **H₆L** (0.04 mmol, 39.0 mg) and **dib** (0.04 mmol, 8.5 mg) in a mixed solvent of dimethylacetamide (DMA, 6 mL) and distilled water (H_2O, 2 mL) were placed in a Teflon-lined

Table 1 Crystallographic data and structure refinement for **1** and **2**

Compound	1	2
CCDC	893227	893228
Empirical formula	$C_{73}H_{89}N_7O_{28}Cd_3$	$C_{84}H_{101}N_9O_{27}Cd_3$
F_w	1849.75	2005.98
Crystal system	Monoclinic	Monoclinic
Space group	$P2_1/c$	$C2/c$
a/Å	24.373(6)	29.766(6)
b/Å	11.367(3)	20.293(5)
c/Å	36.596(10)	16.483(4)
α/°	90	90
β/°	97.685(4)	111.107(4)
γ/°	90	90
V/Å³	10048(5)	9288(4)
z	4	4
T, K	273(2)	
λ (Mo Kα), Å	0.71073	
$F(000)$	3568	3032
Crystal size (mm^3)	$0.12 \times 0.10 \times 0.08$	$0.12 \times 0.11 \times 0.08$
ρ_{calcd} (g cm^{-3})	1.161	1.084
μ (Mo Kα), mm^{-1}	0.691	0.732
R_1/wR_2 ($I > 2\sigma(I)$)^a	0.0775/0.2250	0.0764/0.2144
R_1/wR_2 (all data)	0.1072/0.2469	0.1379/0.2603

^{a} $R_1 = \sum\|F_o| - |F_c\|/\sum|F_o|$, w$R_2 = \{\sum w[(F_o)^2 - (F_c)^2]^2/\sum w[(F_o)^2]^2\}^{1/2}$.

23202 | *J. Mater. Chem.*, 2012, **22**, 23201–23209

This journal is © The Royal Society of Chemistry 2012

Table 2 Bond lengths [Å] and angles [°] for **1** and **2**^{a}

Compound **1**

Cd(1)–O(8)	2.517(5)	Cd(1)–O(9)	2.345(5)
Cd(1)–O(12)#1	2.247(5)	Cd(1)–O(17)#2	2.250(5)
Cd(1)–O(20)	2.303(6)	Cd(1)–O(2W)	2.274(5)
Cd(2)–O(9)	2.315(5)	Cd(2)–O(14)	2.210(5)
Cd(2)–O(13)#1	2.245(5)	Cd(2)–O(16)#2	2.220(5)
Cd(2)–O(10)#3	2.325(5)	Cd(2)–O(18)#1	2.329(6)
Cd(3)–O(15)	2.207(7)	Cd(3)–O(21)	2.427(12)
Cd(3)–O(18)#1	2.492(6)	Cd(3)–O(19)#1	2.303(5)
Cd(3)–O(10)#3	2.336(6)	Cd(3)–O(11)#3	2.634(7)
Cd(3)–O(1W)	2.228(8)		
O(12)#1–Cd(1)–O(20)	92.5(2)	O(12)#1–Cd(1)–O(17)#2	90.7(2)
O(17)#2–Cd(1)–O(20)	171.4(2)	O(12)#1–Cd(1)–O(2W)	100.6(2)
O(12)#1–Cd(1)–O(9)	117.24(19)	O(17)#2–Cd(1)–O(2W)	86.5(2)
O(17)#2–Cd(1)–O(9)	92.3(2)	O(2W)–Cd(1)–O(20)	85.1(2)
O(2W)–Cd(1)–O(9)	142.1(2)	O(12)#1–Cd(1)–O(8)	170.01(19)
O(20)–Cd(1)–O(9)	93.3(2)	O(17)#2–Cd(1)–O(8)	91.1(2)
O(2W)–Cd(1)–O(8)	89.3(2)	O(9)–Cd(1)–O(8)	52.87(17)
O(20)–Cd(1)–O(8)	87.0(2)	O(14)–Cd(2)–O(16)#2	97.2(2)
O(16)#2–Cd(2)–O(13)#1	88.8(2)	O(14)–Cd(2)–O(13)#1	172.4(2)
O(14)–Cd(2)–O(9)	93.5(2)	O(13)#1–Cd(2)–O(9)	81.25(19)
O(16)#2–Cd(2)–O(9)	95.4(2)	O(14)–Cd(2)–O(10)#3	90.0(2)
O(13)#1–Cd(2)–O(10)#3	84.8(2)	O(16)#2–Cd(2)–O(10)#3	168.9(2)
O(9)–Cd(2)–O(10)#3	92.6(2)	O(16)#2–Cd(2)–O(18)#1	87.0(2)
O(14)–Cd(2)–O(18)#1	87.9(2)	O(13)#1–Cd(2)–O(18)#1	97.1(2)
O(9)–Cd(2)–O(18)#1	177.1(2)	O(1W)–Cd(3)–O(10)#3	107.2(3)
O(10)#3–Cd(2)–O(18)#1	84.9(2)	O(19)#1–Cd(3)–O(10)#3	118.2(2)
O(15)–Cd(3)–O(1W)	106.7(3)	O(15)–Cd(3)–O(21)	73.5(4)
O(15)–Cd(3)–O(19)#1	132.2(3)	O(1W)–Cd(3)–O(21)	77.3(4)
O(1W)–Cd(3)–O(19)#1	105.5(3)	O(1W)–Cd(3)–O(18)#1	158.1(3)
O(15)–Cd(3)–O(10)#3	84.2(3)	O(19)#1–Cd(3)–O(18)#1	53.76(18)
O(19)#1–Cd(3)–O(21)	80.3(3)	O(10)#3–Cd(3)–O(18)#1	81.07(18)
O(10)#3–Cd(3)–O(21)	157.5(4)	O(19)#1–Cd(3)–O(11)#3	88.5(2)
O(15)–Cd(3)–O(18)#1	94.2(3)	O(10)#3–Cd(3)–O(11)#3	52.6(2)
O(21)–Cd(3)–O(18)#1	103.0(4)	O(21)–Cd(3)–O(11)#3	146.6(4)
O(15)–Cd(3)–O(11)#3	133.4(3)	O(18)#1–Cd(3)–O(11)#3	95.1(2)
O(1W)–Cd(3)–O(11)#3	75.6(3)		

Compound **2**

Cd(1)–O(6)	2.219(5)	Cd(1)–O(6)#1	2.219(5)
Cd(1)–O(8)#2	2.274(6)	Cd(1)–O(8)#3	2.274(6)
Cd(1)–O(9)#4	2.307(6)	Cd(1)–O(9)#5	2.307(6)
Cd(2)–O(5)	2.158(6)	Cd(2)–O(7)#2	2.508(6)
Cd(2)–O(8)#2	2.307(7)	Cd(2)–O(9)#4	2.490(6)
Cd(2)–O(10)#4	2.259(6)	Cd(2)–N(1)	2.205(7)
O(6)#1–Cd(1)–O(6)	180.0(3)	O(6)–Cd(1)–O(9)#4	89.9(2)
O(6)#1–Cd(1)–O(8)#2	92.8(2)	O(8)#2–Cd(1)–O(9)#4	81.7(2)
O(6)–Cd(1)–O(8)#2	87.2(2)	O(8)#3–Cd(1)–O(9)#4	98.3(2)
O(6)#1–Cd(1)–O(8)#3	87.2(2)	O(6)#1–Cd(1)–O(9)#5	89.9(2)
O(6)–Cd(1)–O(8)#3	92.8(2)	O(6)–Cd(1)–O(9)#5	90.1(2)
O(8)#2–Cd(1)–O(8)#3	180.0(3)	O(8)#2–Cd(1)–O(9)#5	98.3(2)
O(6)#1–Cd(1)–O(9)#4	90.1(2)	O(8)#3–Cd(1)–O(9)#5	81.7(2)
O(9)#4–Cd(1)–O(9)#5	180.0(4)	O(5)–Cd(2)–N(1)	92.0(3)
O(5)–Cd(2)–O(10)#4	135.6(3)	N(1)–Cd(2)–O(8)#2	131.4(3)
N(1)–Cd(2)–O(10)#4	108.1(3)	O(10)#4–Cd(2)–O(8)#2	101.3(3)
O(5)–Cd(2)–O(8)#2	93.1(2)	O(5)–Cd(2)–O(9)#4	88.6(2)
O(10)#4–Cd(2)–O(9)#4	55.0(2)	N(1)–Cd(2)–O(9)#4	151.2(3)
O(10)#4–Cd(2)–O(7)#2	92.0(3)	O(8)#2–Cd(2)–O(9)#4	77.2(2)
O(8)#2–Cd(2)–O(7)#2	53.8(2)	O(5)–Cd(2)–O(7)#2	129.2(3)
O(9)#4–Cd(2)–O(7)#2	114.6(2)	N(1)–Cd(2)–O(7)#2	86.9(3)
O(5)–Cd(2)–C(26)#4	114.1(3)	N(1)–Cd(2)–C(26)#4	132.6(3)

^{a} Symmetry transformations used to generate equivalent atoms: for **1**; #1 x, $-y + 1/2$, $z + 1/2$; #2 $-x$, $-y + 1$, $-z + 2$; #3 $-x + 1$, $-y + 1$, $-z + 2$. For **2**: #1 $-x + 3/2$, $-y + 1/2$, $-z + 1$; #2 x, y, $z - 1$; #3 $-x + 3/2$, $-y + 1/2$, $-z + 2$; #4 $x + 1/2$, $-y + 1/2$, $z - 1/2$; #5 $-x + 1$, y, $-z + 3/2$.

stainless steel vessel (20 mL) and heated to 100 °C for three days; and then cooled to room-temperature slowly. The resulting colorless crystals were obtained after being washed by distilled water, yield 39.4 mg (65% based on Cd^{2+}) for **2**. Its purity was also confirmed by X-ray powder diffraction (XRD). Anal. calcd (%) for **2** $C_{84}H_{101}N_9O_{27}Cd_3$ ($M_r = 2005.98$): C, 50.29; H, 5.07; N, 6.28. Found: C, 50.60; H, 5.16; N, 6.53.

2.3 X-ray crystal structure determination

Suitable single crystals with dimensions of $0.4 \times 0.35 \times 0.32$ mm³ for **1** and $0.32 \times 0.26 \times 0.25$ mm³ for **2** were selected for single-crystal X-ray diffraction analyses. Crystallographic data were collected at 293 K on a Bruker Apex II CCD diffractometer with graphite monochromated Mo-Kα radiation ($\lambda = 0.71073$ Å). Data processing was accomplished with the SAINT program. The structure was solved by direct methods and refined on F^2 by full-matrix least squares using SHELXTL-97.[15] All non-hydrogen atoms except for disordered solvent molecules in **1** were refined with anisotropic displacement parameters during the final cycles. All hydrogen atoms of the organic molecule were placed by geometrical considerations and were added to the structure factor calculation. The formula for **1** and **2** were determined by combining single-crystal structure, elemental microanalysis and TGA. A summary of the crystallographic data for complexes **1** and **2** is listed in Table 1. Selected bond distances and angles are given in Table 2.

2.4 Sorption measurements

The sorption isotherm for N_2 gas and H_2 gas was performed on ASAP 2020 and Autosorb MP-1 apparatuses at 77 K. Prior to the measurement, these as-synthesized samples of **1** and **2** were immersed in methanol for 3 days; during the exchange the methanol was refreshed three times. The resulting methanol-exchanged sample of **1** was transferred as a suspension to a Buchner funnel and the solvent was decanted. The wet sample was then evacuated (10^{-3} torr) at room temperature for 10 h. Obtained samples were immersed in dichloromethane for 12 h, during which the activation solvent was replenished three times. The wet sample was then evacuated (10^{-3} torr) at room temperature for 12 h to remove the solvated molecules. Samples for **2** were further dried at 80 °C under high vacuum for 12 h. Low-pressure gas adsorption experiments were carried out on a Micromeritics ASAP 2020 surface area and pore size analyzer. The BET surface area was calculated from a line regression plot of $1/(W((P_0/P) - 1))$ versus P/P_0 (where W is the total volume absorbed at particular P/P_0 point and P_0 is 1 atm pressure) within the range of $0.02 < P/P_0 < 0.25$.

2.5 Fluorescence measurements

The fluorescence properties of **1** and **2** were investigated in the solid state and in different solvent emulsions at room temperature. The photoluminescent (PL) spectra were recorded on a Hitachi F-4500 fluorescence spectrophotometer. The photomultiplier tube (PMT) voltage was 700 V, the scan speed was 1200 nm min⁻¹ and the slit width of excitation and emission was 2.5 nm. Before the measurements, complex **1** was evacuated under a high vacuum overnight and complex **2** was treated at

80 °C under high vacuum overnight to remove the uncoordinated solvent molecules and to yield the partially activated **1a** and **2a**, respectively. These **1a** and **2a** solvent emulsions were prepared by introducing 3 mg of **1a** and **2a** powder into 5.00 mL of methanol, ethanol, 1-propanol (1-PA), 2-propanol (2-PA), acetone, acetonitrile, dichloromethane (CH_2Cl_2), chloroform ($CHCl_3$), DMF, or tetrahydrofuran (THF). Different amounts of acetone were added into a standard **1a** and **2a** emulsion in 1-propanol, while the concentration of Cd^{2+} was kept constant. To obtain the PL spectra, the **1a** and **2a** solvent emulsions were treated by ultra-sonication for 30 min and then aged for 3 days to form stable emulsions before fluorescence study.

3 Results and discussion

3.1 Structure description

Solvothermal reaction of the semi-rigid ligand **H₆L** with $Cd(NO_3)_3 \cdot 4H_2O$ in mixed DMF–H_2O solution ($v:v = 6:1$) afforded compound **1** as brick-like crystals in good yields. When the rigid ligand **dib** was used as auxiliary bridging ligands in a 8 mL mixed DMA/H_2O solution ($v:v = 3:1$), prism-like crystals of **2** were isolated in good yields. The measured and simulated XRD patterns of the bulk material **1** and **2** are in good agreement with each other, confirming the phase purity of the as-synthesized products (Fig. 1). The two compounds were formulated as $\{[Cd_3(L)(H_2O)_2(DMF)_2] \cdot 5DMF\}_n$ (**1**) and $\{[Cd_3(L)(dib)] \cdot 3H_2O \cdot 5DMA\}_n$ (**2**) based on elemental analysis, single-crystal X-ray diffraction and TGA.

Single crystal X-ray diffraction study reveals that compound **1** crystallizes in a monoclinic space group $P2_1/c$. There are three unique Cd^{2+} ions, one **L⁶⁻** ligand, two aqua ligands and two coordinated DMF molecules in its asymmetric unit (Fig. 2). Cd(1) is six-coordinated in a distorted octahedral geometry by four oxygen atoms from three different **L⁶⁻** anions, one aqua oxygen atom and one coordinated DMF molecule. Cd(2) atom is coordinated by six *trans*-related carboxylate oxygen atoms from four different **L⁶⁻** anions in an octahedral geometry. Cd(3) is coordinated by seven oxygen atoms from three different carboxylate groups, one aqua and one DMF molecule. Cd–O distances range from 2.207(7) Å to 2.634(7) Å. Cd(2)O₆ octahedron connects to two neighboring Cd(1)O₆ and Cd(3)O₇ polyhedra *via* corner- and edge-sharing to form a trinuclear cluster. As seen in Fig. 3, such trimetallic secondary building units (SBUs) are linked by **L⁶⁻** ligands to form a 3D framework with four types of 1-dimensional (1D) channels along the *b*-axis (12.58×8.41 Å², 9.81×7.71 Å², 8.72×8.31 Å² and 8.14×7.83 Å²). The high-solvent-accessible volume of 3057.1 Å³ out of the 10048.0 Å³ unit cell volume (30.4% of the total crystal volume), calculated by PLATON,[16] and the moderate and different pore sizes indicating such 1D channels can be accessible to a variety of small molecules. TOPOS analysis reveals that this framework is a 4,4-connected **sra** net with point symbol of ($4^2 \cdot 6^3 \cdot 8$), where both the metallic SBU and **H₆L** ligand are considered as 4-connected nodes.

The asymmetric unit of **2** contains one and a half Cd^{2+} ions, a half carboxylic ligand and a half **dib** ligand. Cd(1) is located at an inversion site and has an octahedral coordination environment surrounded by six oxygen atoms from four different carboxylate
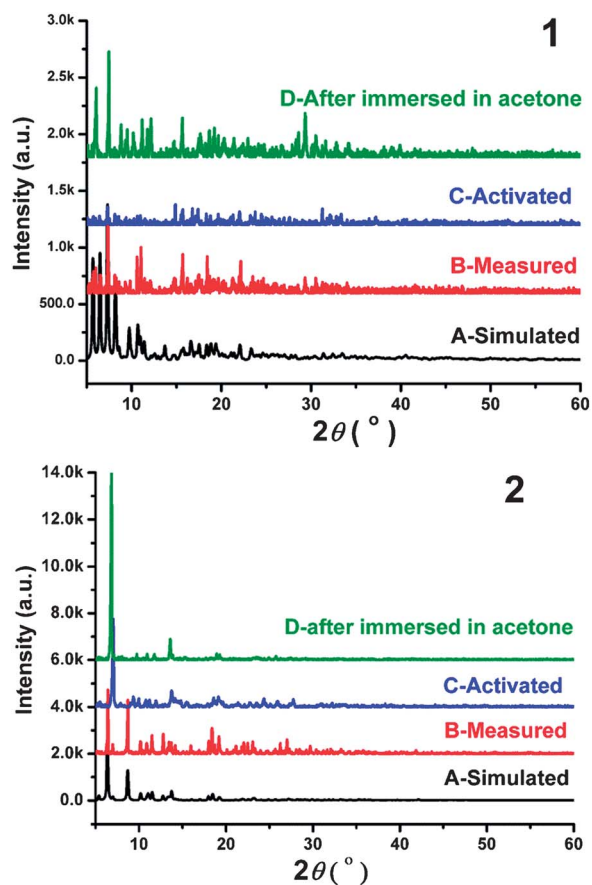
Fig. 1 Powder X-ray diffraction patterns of **1** and **2**.

Fig. 3 The 3D porous framework for **1**. CdO$_x$ ($x = 6$, 7) polyhedra are shaded in gold. Carbon and nitrogen atoms are shown as blue sticks. DMF molecules and hydrogen atoms are omitted for clarity. Right: the simplified **sra** net of **1**.

groups resulting in 2-dimensional (2D) sheets extending along the (010) direction, which are pillared by nitrogen atoms from **dib** ligands to form a 3D framework with large 1D channels (20.60 × 9.96 Å^2 and 10.40 × 9.85 Å^2) along the (001) direction. Based on the calculations using the PLATON program,[16] the total potential solvent accessible void volume is ∼4178.7 Å^3 per unit cell and the pore volume ratio is 45.0%. The detailed crystal information is presented in Tables 1 and 2.

Because of the existence of such large channels (20.60 × 16.87 Å^2) in the single net, it favors constructions of inter-penetrating frameworks inside the void space to stabilize the whole structure. The structure of **2** comprises two-fold inter-penetration (Fig. 5). As we know, in interpenetrating frameworks it is easy to reduce the void space, however, the pore volume ratio (45%) of **2** is higher than that of **1** (35%). It demonstrates that the dual-ligand strategy (flexible and rigid) increases the void space; it plays a key role in geometrical and structural complementary, as well as strengthens and directs the framework, so a dual-ligand strategy is effective to eliminate the defect of the interpenetrating framework. Interpenetrating enhances the stability of frameworks and improves gas separation and storage abilities.

ligands (Fig. 4). Cd(2) is coordinated by five oxygen atoms from three **L**$^{6-}$ anions and one terminal nitrogen atom. Three Cd atoms are bridged into a linear trimer *via* edge-sharing. These trinuclear clusters are further linked together by the carboxylate

Fig. 2 An ORTEP representation of the asymmetric units of **1**. Thermal ellipsoids are drawn at the 50% probability level (Cd, green; carbon, gray; nitrogen, blue; oxygen, red) and the hydrogen atoms are omitted for clarity.
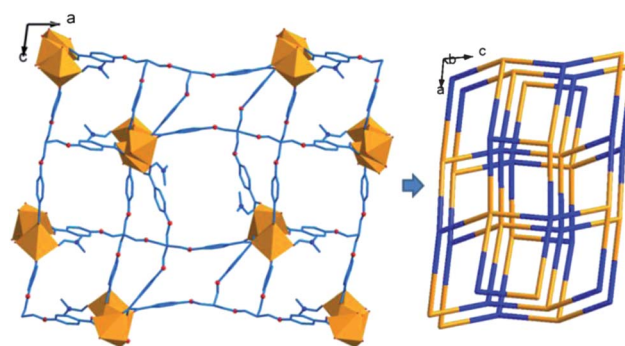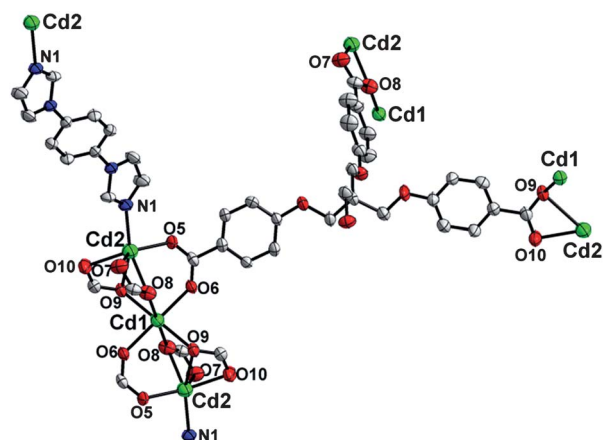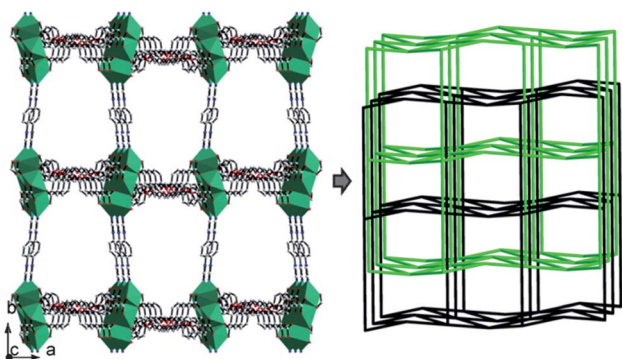

Fig. 4 An ORTEP representation of the asymmetric units of **2** giving the trimetallic SBU (Cd, green; carbon, gray; nitrogen, blue; oxygen, red). Thermal ellipsoids are drawn at the 50% probability level and the hydrogen atoms are omitted for clarity.

This journal is © The Royal Society of Chemistry 2012

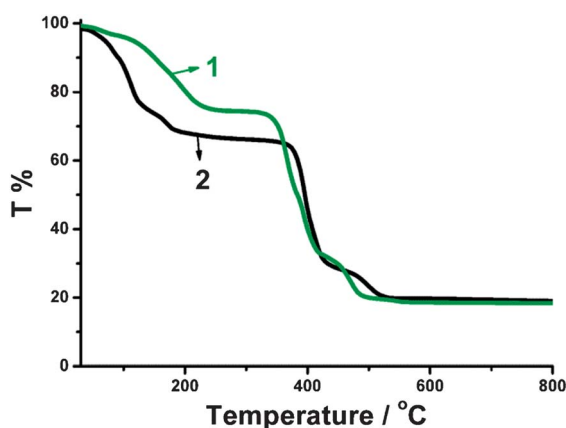*J. Mater. Chem.*, 2012, **22**, 23201–23209 | 23205

Fig. 5 One independent single net in the interpenetrating framework of **2** (Cd, green; carbon, gray; nitrogen, blue; oxygen, red). Hydrogen atoms are omitted for clarity. Right side: the simplified 2-fold interpenetrating networks of **2**.

3.2 Thermal stabilities

The TGA of compounds **1** and **2** were carried out, as shown in Fig. 6. The TGA diagrams of the two compounds are quite similar and both show two main weight losses in the curves. For **1**, the first step (46–180 °C) corresponds to the release of five DMF molecules, two coordinated DMF molecules and two aqua ligands. The observed weight loss of 31.4% is larger than the calculated values (29.6%) and that may be due to the water molecules of surface adsorption. The second weight loss of 46.0% between 338 °C and 548 °C is attributed to the loss of the ligand composite. The total observed weight loss is 80.2% at 548 °C. The TGA result of **2** reveals a gradual weight loss of 25.1% in the temperature range of 46–261 °C corresponding to the release of solvent molecules incorporated into the pores (3.0 equiv. of H_2O and 5 equiv. of DMA per formula unit). The guest-free framework is stable up to 321 °C, followed by a collapse upon further calculation. The total observed weight loss is 81.3% at 560 °C. The final residuals for the two compounds were not characterized due to their corrosive reactions with the TGA buckets made of Al_2O_3, however it is expected to be mainly cadmium(II) oxide.

Based on the high stability of **2**, the robustness and the permanent microporous feature of the activated **2a** (activated at 80 °C under high vacuum for 24 h) was further established by N_2
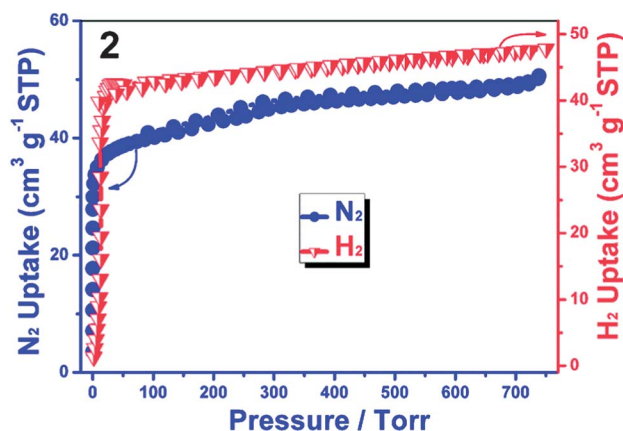
Fig. 7 Gas sorption isotherms of compound **2**.

sorption isotherm at 77 K, which displays typical type-I sorption behavior (Fig. 7). It takes up 141 cm^3 g^{-1} of N_2 at 77 K and 1 atm. The calculated Langmuir and BET surface areas are 178 and 138 m^2 g^{-1}, respectively. The H_2 uptake at 77 K reached 47.8 cm^3 g^{-1} in 1 atm. An average pore size of 2.23 nm was calculated. The activated **1a** (activated at 80 °C under a high vacuum for 24 h) has lost its framework, so un-activated **1** was used for gas adsorption, whereas un-activated **1** takes up negligible amounts of nitrogen and hydrogen, indicating channels in the framework are extremely small (filled by solvent molecules) to allow the incorporation of N_2 or H_2.
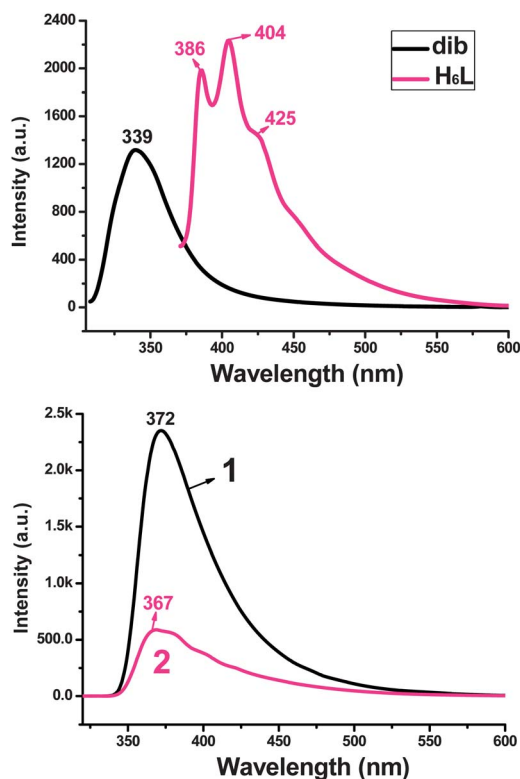
3.3 Luminescence properties

Metal–organic frameworks constructed from d^{10} metal ions and various organic ligands are commonly reported compared with other transition metal ions because the d^{10} metal ions not only display varied coordination numbers and geometries, but also exhibit luminescent properties. As a result, they are promising candidates for potential photoactive materials. The dual-ligand approach by the judicious choice of organic linkers is effective to construct novel topological MOFs. It is necessary to further investigate the influence of different structural features on luminescence properties.
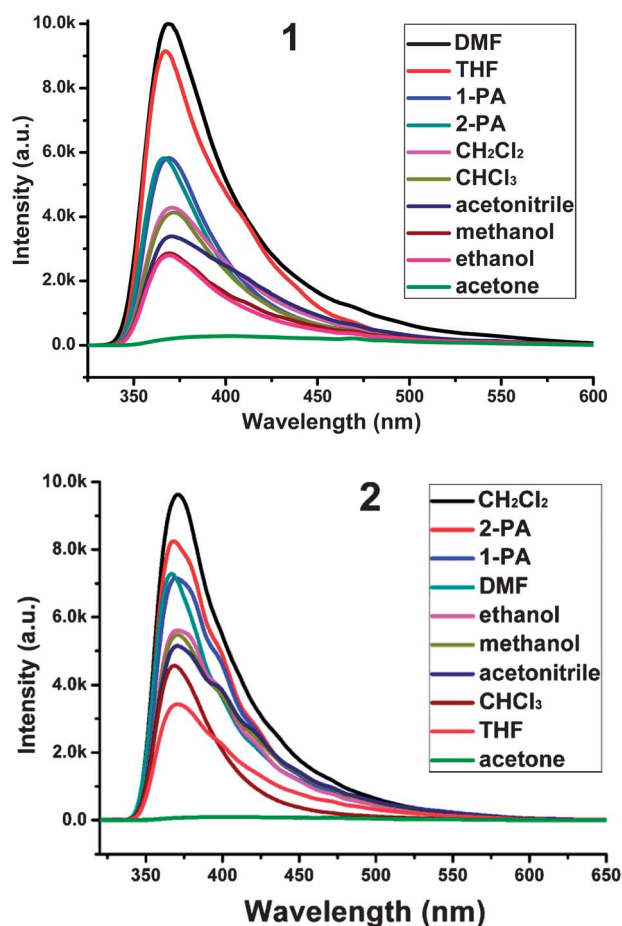
The solid luminescence spectrum of ligand **H_6L**, **dib**, the activated phase **1a** and **2a** at room temperature are shown in Fig. 8 . The free **H_6L** displays two main fluorescent emission bands at $\lambda_{max} = 386$, 404 nm and one shoulder peak at $\lambda_{max} = 425$ nm under excitation at 351 nm. Upon its complexation with metal ions, **1a** exhibits one strong peak at $\lambda_{max} = 372$ nm under excitation at 299 nm. **2a** also shows the ligand-based fluorescence emission band locating at around 367 nm upon excitation at 292 nm, in which the coefficient of carboxylate ligand and **dib** with metal centers contribute to the fluorescent emission.

As mentioned above, the different 1D channels of **1** and **2** are filled by a large number of solvent molecules. The robustness and the permanent micropore feature of the activated **1a** and **2a** have been demonstrated by gas adsorption and TGA. Considering the intrinsic structural property, it is anticipated that the solvent molecules could be replaced by other different common organic solvents. In this regard, to examine the potential sensing of small solvent molecules, the fluorescence properties of **1a** and **2a** in

Fig. 6 Thermogravimetric analyses of **1** and **2**.

23206 | *J. Mater. Chem.*, 2012, **22**, 23201–23209

This journal is © The Royal Society of Chemistry 2012

different solvent emulsions were investigated. As shown in Fig. 9, the PL spectra are similar to the solid state ones. The predominant feature is that the PL intensities are largely dependent on the solvent molecules, particularly in the case of acetone, which exhibits the most quenching behavior and the most enhancing effects, observed in DMF and 2-propanol for **1a** and **2a**, respectively (Fig. S2†). To examine sensing sensitivity toward acetone in detail, a batch of emulsions of **1a** or **2a** dispersed in 1-PA solution with gradually increasing acetone contents were prepared to monitor the emissive response. A gradual decrease of the fluorescence intensity was observed upon the addition of acetone to the 1-PA emulsion of **1a** and **2a** (Fig. 10). The fluorescence decrease was nearly proportional to the acetone concentration. The decreasing trend of the fluorescence intensity at 372 nm for **1a** and 367 nm for **2a** *versus* the volume ratio of acetone could be well fitted with a first-order exponential decay (Fig. 11), indicating that fluorescence quenching of **1a** and **2a** by acetone is diffusion-controlled.[5] As shown in Fig. 10, the luminescence intensity has decreased to 50% at an acetone content of 0.3 vol% for **1a** and **2a**, and was almost completely quenched at a concentration of 1.0 vol% for **1a** and 2.0 vol% for **2a**, thus the compounds reported in this paper can be seen as candidates for selective sensing of acetone. The physical interaction of the solute and solvent plays an important role in such fluorescence enhancing and quenching effects of small solvent molecules. Upon excitation, there is a competition of absorption of the light source energy between the solvent molecules and organic ligands. The energy absorbed by the organic ligands is transferred to
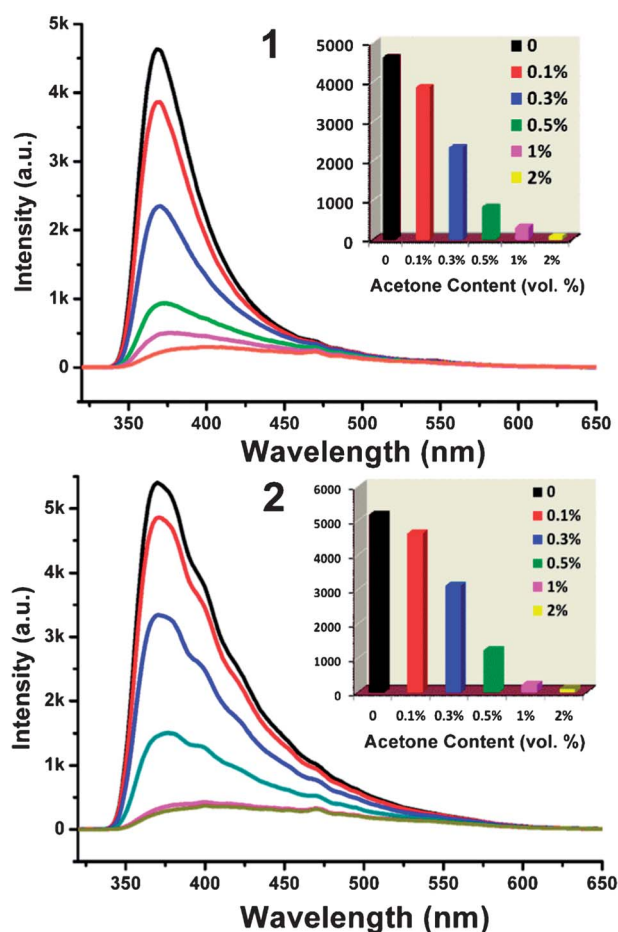

Fig. 9 PL spectra of **1a** and **2a** introduced into various pure solvents when excited at 299 nm and 292 nm, respectively.

acetone molecules, resulting in a decrease in the luminescence intensity.[5]

4 Conclusions

In summary, one new Cd-MOF (**1**) was synthesized based on a semi-rigid hexavalent acid. The dispersed solution of particles of **1** in acetone displays highly sensitive fluorescence quenching behavior. Introducing a rigid N-donor ligand (**dib**), microporous Cd-MOF (**2**) was obtained, which exhibits similar excellent luminescence sensing in acetone, except that it shows higher stability and larger pore size. As a result, the dual-ligand strategy is effective in constructing new MOFs with different pore sizes, which make MOFs good candidates for separation and sensing small molecules. Two microporous luminescent Cd-MOFs (**1** and **2**) illustrate unprecedented sensing and detection properties by the fluorescent quenching method. Such a quenching mechanism is due to a competition of adsorption of the light source energy between the excited MOF and acetone molecules adsorbed in the pores and on the surface of the MOF particles. More importantly, it is the first report that Cd-MOFs have excellent luminescence sensing ability for acetone molecules. They could be potential luminescent probes. It is expected that more microporous luminescent sensing MOFs will emerge in the future.

Fig. 8 Solid-state emission spectra of ligands **H$_6$L** (pink, λ_{ex} = 351 nm) and **dib** (black, λ_{ex} = 288 nm), the activated phase **1a** (black, λ_{ex} = 299 nm) and **2a** (pink, λ_{ex} = 292 nm).

Fig. 10 PL spectra of the dispersed MOFs (**1** and **2**) in 1-propanol in the presence of various contents of acetone solvent (excited at 299 nm and 292 nm, respectively). Inset: corresponding emission intensities.
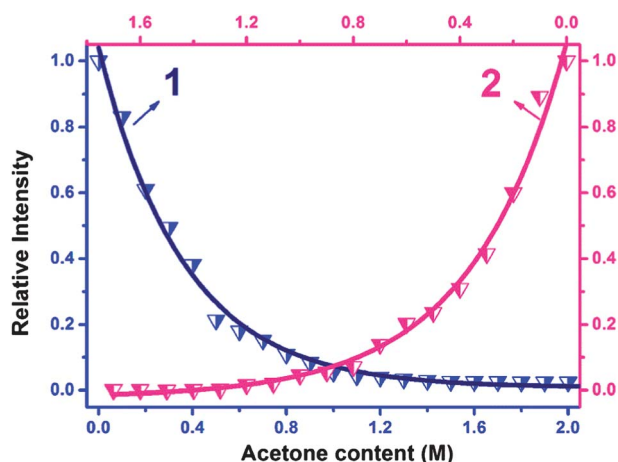
Fig. 11 The luminescence intensity of the Cd-MOFs (**1a** and **2a**) 1-propanol suspension as a function of acetone content.

Acknowledgements

Notes and references

1 (*a*) J. M. García, F. C. García, F. Serna and J. L. D. L. Peña, *Polym. Rev.*, 2011, **51**, 341–390; (*b*) Y. Salinas, R. Martínez-Máñez, M. D. Marcos, F. Sancenón, A. M. Costero, M. Parraad and S. Gilad, *Chem. Soc. Rev.*, 2012, **41**, 1261–1296; (*c*) S. W. Thomas, G. D. Joly and T. M. Swager, *Chem. Rev.*, 2007, **107**, 1339–1386; (*d*) N. M. Bergmann and N. Peppas, *Prog. Polym. Sci.*, 2008, **33**, 271–288.

2 (*a*) B. N. Chen, S. Piletsky and A. P. F. Turner, *Comb. Chem. High Throughput Screening*, 2002, **5**, 409–427; (*b*) L. Ding and Y. Fang, *Chem. Soc. Rev.*, 2010, **39**, 4258–4273; (*c*) J. Homola, *Chem. Rev.*, 2008, **108**, 462–493; (*d*) J. López-Gejo, A. Arranz, Á. Navarro, C. Palacio, E. Muñoz and G. Orellana, *J. Am. Chem. Soc.*, 2010, **132**, 1746–1747.

3 (*a*) A. Prasanna de Silva, H. Q. Nimal Gunaratne, T. Gunnlaugsson, A. J. M. Huxley, C. P. McCoy, J. T. Rademacher and T. E. Rice, *Chem. Rev.*, 1997, **97**, 1515–1566; (*b*) L. Basabe-Desmonts, D. N. Reinhoudt and M. Crego-Calama, *Chem. Soc. Rev.*, 2007, **36**, 993–1017; (*c*) B. L. Chen, L. B. Wang, Y. Q. Xiao, F. R. Fronczek, M. Xue, Y. J. Cui and G. D. Qian, *Angew. Chem., Int. Ed.*, 2009, **48**, 500; (*d*) Y. Cui, Y. Yue, G. Qian and B. Chen, *Chem. Rev.*, 2012, **112**, 1126–1162; (*e*) A. J. Lan, K. H. Li, H. H. Wu, D. H. Olson, T. J. Emge, W. Ki, M. C. Hong and J. Li, *Angew. Chem., Int. Ed.*, 2009, **48**, 2334; (*f*) Z. G. Xie, L. Q. Ma, K. E. deKrafft, A. Jin and W. B. Lin, *J. Am. Chem. Soc.*, 2010, **132**, 922.

4 (*a*) C. J. Cumming, C. Aker, M. Fisher, M. Fox, M. J. la Grone, D. Reust, M. G. Rockley, T. M. Swager, E. Towers and V. Williams, *IEEE Trans. Geosci. Remote Sens.*, 2001, **39**, 1119–1128; (*b*) S. J. Toal and W. C. Trogler, *J. Mater. Chem.*, 2006, **16**, 2871–2883.

5 (*a*) Z. Guo, H. Xu, S. Su, J. Cai, S. Dang, S. Xiang, G. Qian, H. Zhang, M. O'Keeffe and B. Chen, *Chem. Commun.*, 2011, **47**, 5551–5553; (*b*) D. Ma, W. Wang, Y. Li, J. Li, C. Daiguebonne, G. Calvezc and O. Guillou, *CrystEngComm*, 2010, **12**, 4372–4377; (*c*) B. Chen, Y. Yang, F. Zapata, G. Lin, G. Qian and E. B. Lobkovsky, *Adv. Mater.*, 2007, **19**, 1693–1696; (*d*) W. Yang, J. Feng and H. Zhang, *J. Mater. Chem.*, 2012, **22**, 6819–6823.

6 (*a*) C. Zhang, Y. Che, Z. Zhang, X. Yang and L. Zang, *Chem. Commun.*, 2011, **47**, 2336–2338; (*b*) H. Xu, F. Liu, Y. Cui, B. Chen and G. Qian, *Chem. Commun.*, 2011, **47**, 3153–3155; (*c*) B. Chen, S. Xiang and G. Qian, *Acc. Chem. Res.*, 2010, **43**, 1115–1124; (*d*) Y. Xiao, Y. Cui, Q. Zheng, S. Xiang, G. Qian and B. Chen, *Chem. Commun.*, 2010, **46**, 5503; (*e*) Z. Zhang, S. Xiang, X. Rao, Q. Zheng, F. R. Fronczek, G. Qian and B. Chen, *Chem. Commun.*, 2010, **46**, 7205.

7 (*a*) T. M. Reineke, M. Eddaoudi, M. Fehr, D. Kelley and O. M. Yaghi, *J. Am. Chem. Soc.*, 1999, **121**, 1651; (*b*) B. Chen, L. Wang, F. Zapata, G. Qian and E. B. Lobkovsky, *J. Am. Chem. Soc.*, 2008, **130**, 6718; (*c*) B. V. Harbuzaru, A. Corma, F. Rey, J. L. Jorda, D. Ananias, L. D. Carlos and J. Rocha, *Angew. Chem., Int. Ed.*, 2009, **48**, 6476; (*d*) K. A. White, D. A. Chengelis, K. A. Gogick, J. Stehoud, N. L. Rosi and S. Petoud, *J. Am. Chem. Soc.*, 2009, **131**, 18069; (*e*) A. J. Lan, K. H. Li, H. H. Wu, L. Z. Kong, N. Nijem, D. H. Olson, T. J. Emge, Y. J. Chabal, D. C. Langreth, M. C. Hong and J. Li, *Inorg. Chem.*, 2009, **48**, 7165; (*f*) S. Pramanik, C. Zheng, X. Zhang, T. J. Emge and J. Li, *J. Am. Chem. Soc.*, 2011, **133**, 4153; (*g*) H. Nie, Y. Zhao, M. Zhang, Y. Ma, M. Baumgarten and K. Müllen, *Chem. Commun.*, 2011, **47**, 1234–1236; (*h*) B. Gole, A. K. Bar and P. S. Mukherjee, *Chem. Commun.*, 2011, 12137.

8 (*a*) H.-L. Jiang, B. Liu, Y.-Q. Lan, K. Kuratani, T. Akita, H. Shioyama, F. Zong and Q. Xu, *J. Am. Chem. Soc.*, 2011, **133**, 11854–11857; (*b*) H.-L. Jiang, Y. Tatsu, Z.-H. Lu and Q. Xu, *J. Am. Chem. Soc.*, 2010, **132**, 5586–5587; (*c*) H.-L. Jiang, B. Liu, T. Akita, M. Haruta, H. Sakurai and Q. Xu, *J. Am. Chem. Soc.*, 2009, **131**, 11302–11303; (*d*) H.-L. Jiang and Q. Xu, *Chem. Commun.*, 2011, **47**, 3351–3370; (*e*) H.-L. Jiang, Q.-P. Lin, T. Akita, B. Liu, H. Ohashi, H. Oji, T. Honma, T. Takei, M. Haruta and Q. Xu, *Chem.–Eur. J.*, 2011, **17**, 78–81.

23208 | *J. Mater. Chem.*, 2012, **22**, 23201–23209

This journal is © The Royal Society of Chemistry 2012

9 (a) H. Furukawa, N. Ko, Y. B. Go, N. Aratani, S. B. Choi, E. Choi, A. O. Yazaydin, R. Q. Snurr, M. O'Keeffe, J. Kim and O. M. Yaghi, *Science*, 2010, **239**, 424–428; (b) J.-R. Li, R. J. Kuppler and H.-C. Zhou, *Chem. Soc. Rev.*, 2009, **38**, 1477–1504; (c) Y.-B. Zhang, W.-X. Zhang, F.-Y. Feng, J.-P. Zhang and X.-M. Chen, *Angew. Chem., Int. Ed.*, 2009, **48**, 5287–5290; (d) M.-H. Zeng, M.-X. Yao, H. Liang, W.-X. Zhang and X.-M. Chen, *Angew. Chem., Int. Ed.*, 2007, **46**, 1832–1835.

10 (a) S.-T. Zheng, J. J. Bu, T. Wu, C. Chou, P. Feng and X. Bu, *Angew. Chem., Int. Ed.*, 2011, **50**, 8858–8862; (b) D. Yuan, D. Zhao, D. Sun and H.-C. Zhou, *Angew. Chem., Int. Ed.*, 2010, **49**, 5357–5361; (c) D. Han, F.-L. Jiang, M.-Y. Wu, L. Chen, Q.-H. Chen and M.-C. Hong, *Chem. Commun.*, 2011, **47**, 9861–9863; (d) L. Ma, C. Abney and W. Lin, *Chem. Soc. Rev.*, 2009, **38**, 1248–1256.

11 (a) D. J. Tranchemontagne, J. L. Mendoza-Cortés, M. O'Keeffe and O. M. Yaghi, *Chem. Soc. Rev.*, 2009, **38**, 1257–1283; (b) H.-C. Zhou, J. Long and O. M. Yaghi, *Chem. Rev.*, 2012, **112**, 673–674; (c) Z. Guo, H. Wu, G. Srinivas, Y. Zhou, S. Xiang, Z. Chen, Y. Yang, W. Zhou, M. O. Keeffe and B. Chen, *Angew. Chem., Int. Ed.*, 2011, **50**, 3178–3181; (d) M. C. Das, S. Xiang, Z. Zhang and B. Chen, *Angew. Chem., Int. Ed.*, 2011, **50**, 10510–10520.

12 (a) H. Li, M. Eddaoudi, M. O'Keeffe and O. M. Yaghi, *Nature*, 1999, **402**, 276–279; (b) M. Eddaoudi, J. Kim, N. Rosi, D. Vodak, J. Wachter, M. O'Keeffe and O. M. Yaghi, *Science*, 2002, **295**, 469–472.

13 (a) Z. Guo, R. Cao, X. Wang, H. Li, W. Yuan, G. Wang, H. Wu and J. Li, *J. Am. Chem. Soc.*, 2009, **131**, 6894–6895; (b) P. K. Thallapally, J. Tian, M. R. Kishan, C. A. Fernandez, S. J. Dalgarno, P. B. McGrail, J. E. Warren and J. L. Atwood, *J. Am. Chem. Soc.*, 2008, **130**, 16842–16843; (c) T. K. Kim and M. P. Suh, *Chem. Commun.*, 2011, **47**, 4258–4260; (d) M. R. Kishan, J. Tian, P. K. Thallapally, C. A. Fernandez, S. J. Dalgarno, J. E. Warren, B. P. McGraila and J. L. Atwood, *Chem. Commun.*, 2010, **46**, 538–540.

14 (a) H.-Y. Wu, R.-X. Wang, W. Yang, J. Chen, Z.-M. Sun, J. Li and H. Zhang, *Inorg. Chem.*, 2012, **51**, 3103–3107; (b) E. M. D. Keegstra, J. W. Zwikker, M. R. Roest and L. W. Jenneskens, *J. Org. Chem.*, 1992, **57**, 6678–6680; (c) Y.-W. Wang, Y.-L. Zhang, W. Dou, A.-J. Zhang, W.-W. Qin and W.-S. Liu, *Dalton Trans.*, 2010, **39**, 9013–9021; (d) D. Laliberte, T. Maris, A. Sirois and J. D. Wuest, *Org. Lett.*, 2003, **5**, 4787–4790; (e) D. Laliberte, T. Maris and J. D. Wuest, *J. Org. Chem.*, 2004, **69**, 1776–1787; (f) J. Cho, T. Keith Hollis, E. J. Valente and J. M. Trate, *J. Organomet. Chem.*, 2011, **696**, 373–377.

15 (a) G. M. Sheldrick, *Program SADABS*, Universität Göttingen, Göttingen, Germany, 1995; *CrystalClear, Version 1.3.5*, Rigaku Corp., Woodlands, TX, 1999; (b) G. M. Sheldrick, *SHELX-96 program for crystal structure Determination*, Siemens Analytical X-ray Instruments, Madison, WI, 1996.

16 (a) A. L. Spek, *Acta Crystallogr., Sect. A: Found. Crystallogr.*, 1990, **46**, 194–201; (b) A. L. Spek, *PLATON99, a Multipurpose Crystallographic Tool*, Utrecht University, Utrecht, The Netherlands, 1999.

This journal is © The Royal Society of Chemistry 2012

J. Mater. Chem., 2012, **22**, 23201–23209 | 23209